Backward erosion piping in geotechnical infrastructure: a rate process perspective

ZHIJIE WANG*, CAGLAR OSKAY† and ALESSANDRO FASCETTI*

Backward erosion piping (BEP) has been recognised as a major cause of failures in water-retaining structures. However, the fundamental mechanisms controlling the phenomenon are not well understood. This research applies the theory of rate processes to develop a constitutive relationship between energy density of the seepage flow and the erosion rate of soils during the evolution of BEP. The resulting equation is used to analyse four datasets of previously reported experimental observations. The mechanical parameters estimated through the proposed model fall into the ranges of values that were reported in the literature. To validate the proposed approach, the constitutive model was incorporated into a multiphase numerical framework to simulate evolution of BEP in embankment soil and compared with reported experimental observations. The numerical framework with the proposed constitutive model is shown to be capable of reproducing both the observed evolution of local hydraulic gradients and pipe progression in the structure.

KEYWORDS: backward erosion piping; constitutive modelling; erosion; flow energy; rate process

INTRODUCTION

Internal erosion is considered to play a leading role in embankment dam failures, as it has been attributed as the cause of approximately one half of embankment failures worldwide (Foster *et al*., 2000). According to the International Commission on Large Dams (ICOLD), there are four types of internal erosion based on their failure mechanisms: suffusion, concentrated leaks, contact erosion and backward erosion (ICOLD, 2013). The properties of the soils in an embankment or in its foundation determine to which of these erosion mechanisms it will be most vulnerable. Suffusion occurs in widely graded or gap-graded cohesionless soils where finer particles are eroded through pores between coarser particles by seepage flow. Concentrated leaks occur in plastic soils, or unsaturated silts and sands, where an opening exists and is enlarged as soil particles are eroded by the leaking water. Contact erosion occurs on the contact interface of a coarser soil, such as a gravel, and a fine soil where flow parallel to the contact in the coarse soil erodes the fine soil. Backward erosion piping (BEP) mainly occurs in embankment foundations of cohesionless soils where soil particles under a roof of cohesive top layer are eroded by the seepage flow, and a pipe initiates at a free unfiltered surface downstream and progresses upstream causing instability of the flood protection system (Robbins, 2016; Vandenboer *et al*., 2018; Pol *et al*., 2022). BEP is the most common mechanism accounting for up to one third of all internal erosion failures of embankment dams and their foundations (Richards & Reddy, 2007). The present study focuses on the development of a novel theoretical framework to describe the evolution of BEP in geotechnical infrastructure.

Owing to the catastrophic consequences of BEP, a considerable amount of research has been focused on assessing the likelihood of BEP in geotechnical flood protection infrastructure (GFPI) systems. Several semi-empirical models have been proposed in the literature to evaluate the potential of BEP based on experimental observations. In these models, a central challenge has been characterising the response of soils under different hydraulic loading conditions, with an emphasis on identifying the critical hydraulic loading that initiates and propagates BEP. Hydraulic gradient and hydraulic shear stress have been proposed as measures to characterise hydraulic loading and constitutive laws have been developed to predict the soil erosion rate revolving around these two quantities. Identification of the critical hydraulic gradient or the critical shear stress for pipe initiation has therefore been widely studied (Bligh, 1910; Sellmeyer, 1988; Reddi *et al*., 2000; Ojha *et al*., 2003; van Beek *et al*., 2010; Fleshman & Rice, 2013; Negrinelli, 2015; van Beek *et al*., 2015; Peng & Rice, 2020). Recently, the flow energy has been proposed as an objective measure to characterise the hydraulic loading intensity. Corresponding constitutive relationships have been developed between erosion rate and flow energy based on experimental observations (Marot *et al*., 2012; Sibille *et al*., 2015; Kodieh *et al*., 2021).

Experimental works available in the literature shed light on the characteristics of BEP and its evolution both at the laboratory (Richards & Reddy, 2012; Fleshman & Rice, 2014; van Beek, 2015; Robbins *et al*., 2018; Ovalle-Villamil and Sasanakul, 2021) and field scales (van Beek *et al*., 2011; Robbins *et al*., 2020; Marchi *et al*., 2021). Current strategies employ semi-analytical methods or simplified schematisation of the field conditions to estimate the potential for piping evolution and to guide the design of new systems as well as the retrofitting of existing ones (Schmertmann, 2000; Sellmeijer *et al*., 2011; Brandon *et al*., 2018). However, the complexity in describing the full breadth of field conditions and GFPI structural arrangements (i.e. variations in geometrical features, spatial variability in soil conditions,

Manuscript received 11 August 2023; revised manuscript accepted 11 March 2024. First published online ahead of print 25 March 2024.
Discussion on this paper is welcomed by the editor.
* Department of Civil and Environmental Engineering, University of Pittsburgh, Pittsburgh, PA, USA.
† Department of Civil and Environmental Engineering, Vanderbilt University, Nashville, TN, USA.

possible presence of filters, upward sloping and pressure relief systems) makes it prohibitive to fully characterise the potential of BEP experimentally. Therefore, mathematical and numerical models are required to estimate the likelihood of failure of the GFPI and inform design strategies.

Numerical approaches, which have been employed in previous studies on BEP, generally fall into three categories: (*a*) single-phase transport models in which the permeability of the soil is increased to simulate the progression of erosion (Vandenboer *et al.*, 2014; Fascetti & Oskay, 2019a; Robbins & Griffiths, 2021); (*b*) discrete-element approaches, generally coupled with continuum descriptions for the fluid flow, to investigate localised phenomena (El Shamy & Aydin, 2008; Wang & Ni, 2013); and (*c*) multiphase models in which the density evolution of mobilised particles is described using regularised constitutive relationships and coupled with the groundwater flow by way of kinematic constraints (Papamichos & Vardoulakis, 2005; Zhang *et al.*, 2013; Fascetti & Oskay, 2019b). The above-mentioned numerical approaches utilise semi-empirical constitutive relationships based on a critical hydraulic gradient or a critical hydraulic shear stress. Moreover, the definition of a critical value of the hydraulic gradient (or tangential shear) is prohibitive in three-dimensional (3D) problems, as the values of such parameters are highly influenced by flow direction and characteristics.

The theory of rate processes is based on statistical mechanisms and has been successfully employed to describe particulate systems undergoing time-dependent flow or deformation (Eyring, 1936; Glasstone *et al.*, 1941). Applications of the theory of rate processes to soil behaviour began in the 1960s (Mitchell, 1964; Mitchell *et al.*, 1968, 1969; Andersland & Douglas, 1970; Christensen & Das, 1973; Raudkivi & Hutchison, 1974; Gularte *et al.*, 1980; Murayama *et al.*, 1984). Among the aforementioned articles, Christensen & Das (1973), Raudkivi & Hutchison (1974) and Gularte *et al.* (1980) dealt with the surface erosion of cohesive soils, while the rest of these studies were focused on either strength or creep of soils. The reported dependencies of erosion rates on temperature and hydraulic shear stress were in agreement with the theory of rate processes (Christensen & Das, 1973; Raudkivi & Hutchison, 1974; Gularte *et al.*, 1980). However, such a theoretical framework has not yet been applied to the internal erosion process in sand, which controls the evolution of BEP.

Therefore, the aim of this study is to propose and evaluate a theoretical model, based on the theory of rate processes, to describe BEP progression in GFPI systems. The model was derived from fundamental inter-granular interactions in cohesionless soils rather than being generalised from phenomenological observations. The central component of the proposed model is a constitutive relationship between the erosion rate of soil mass in time and the energy density of seepage flow. The constitutive relationship is first exercised to perform non-linear regressions on four experimental internal erosion datasets reported in the literature. The mechanical parameters estimated from the regressions are in good agreement with those reported in previous studies. To illustrate its capability in describing the progression of BEP in GFPI, the proposed model was incorporated into a multiphase numerical framework, and simulation results were compared to reported experimental outcomes. The numerical results demonstrate that the model is capable of representing both the global BEP progression rates and local hydraulic conditions around the pipe tip. Moreover, the estimated mechanical parameters are consistent with each other and align with previously reported values for different mechanisms. To the best of the authors' knowledge, this work represents the first attempt to utilise the theory of rate processes to describe BEP.

BEP AS A RATE PROCESS

Based on review of experiments available in the literature at the small, medium and large scale, BEP in geotechnical systems (see Fig. 1) exhibits the following traits: (*a*) stochasticity; (*b*) complex dynamic equilibrium conditions that yield 'step-wise' behaviour (see Fig. 2); and (*c*) some degree of exponential acceleration of the phenomenon when the intact portion of the system (i.e. the upstream side not yet subjected to erosion) is reduced to approximately 1/3 of the seepage length (van Beek *et al.*, 2015). These traits lead us to

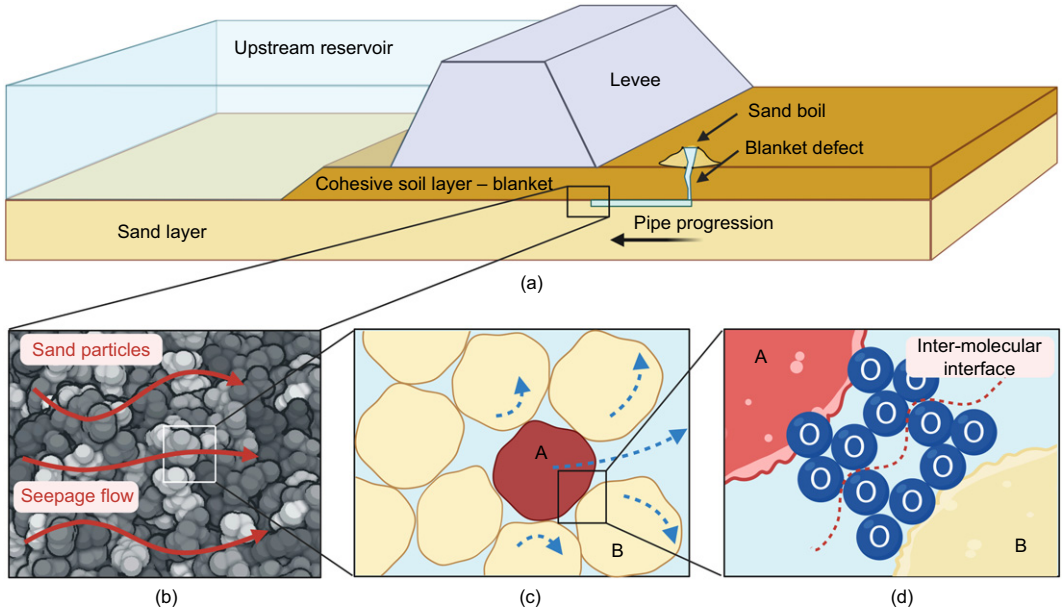

Fig. 1. Schematic representation of mechanisms of BEP at multiple scales (created with BioRender.com): (a) concept of BEP development; (b) sand particles and seepage flow; (c) erosion of a sand particle through progressive structural rearrangements; (d) actual inter-particle contact at molecular scale

cast a parallelism with the theory of rate processes, in which an explicit consideration of a free energy barrier is derived that guides the evolution of the process in exam. Glasstone *et al.* (1941) pointed out that the theory of rate processes is not only a theory of kinetics of chemical reactions, but also one that can be applied to any process involving a rearrangement of matter – that is, a 'rate process'. In fact, the theory of rate processes has been successfully used in describing different physical mechanisms in soils, such as creep, shear deformation and surface erosion of clays (Mitchell, 1964; Mitchell *et al.*, 1968; Gularte *et al.*, 1980). In this study, the application of the theory of rate processes to BEP in cohesionless soils is investigated to provide insights into the fundamental nature of BEP and development of new analytical and numerical frameworks. Detailed development of the theory of rate processes may be found in Eyring (1936), Glasstone *et al.* (1941) and other works in the physical chemistry literature.

The theory of rate processes idealises atoms, molecules and/or particles participating in a flow (or deformation) process, termed flow units, as constrained from movement relative to each other by energy barriers which separate adjacent equilibrium positions. The displacement of one mole of flow units to new positions requires the expenditure of an activation energy ΔF to surmount the barrier (see Fig. 3). The energy expended for a flow unit to cross a barrier may be provided by thermal energy and by various applied potentials. For a material at rest, the potential energy–displacement relationship is represented as curve A in Fig. 3. The number of times that a given unit is activated, or the proportion of a certain number of flow units that are activated, v, per second is given by (frequency of activation):

$$v = \frac{k_b T}{h_p} \exp\left(-\frac{\Delta F}{RT}\right) \tag{1}$$

where k_b is the Boltzmann's constant ($1{\cdot}38 \times 10^{-23}$ J/K); T is the absolute temperature (K); h_p is the Planck's constant ($6{\cdot}624 \times 10^{-34}$ J/s); and R is the universal gas constant ($8{\cdot}3144$ J/(K/mol)).

In the absence of directional potentials, flow units are oscillating across the barriers at equal frequency in all directions, generating no net directional flow. However, if a directed potential, such as a force, f, is applied, then the barrier heights are shifted as shown by curve B in Fig. 3. The barrier height in the direction of the force is reduced and the activation frequency to the right is

$$v \rightarrow = \frac{k_b T}{h_p} \exp\left(-\frac{\Delta F}{RT} + \frac{f\lambda}{2k_b T}\right) \tag{2}$$

and the frequency to the left is

$$v \leftarrow = \frac{k_b T}{h_p} \exp\left(-\frac{\Delta F}{RT} - \frac{f\lambda}{2k_b T}\right) \tag{3}$$

where $R = k_b N$ and N is the Avogadro constant ($6{\cdot}022 \times 10^{23}$); and λ represents the distance between successive equilibrium positions. Therefore, the net frequency or probability of activation towards the direction of the force direction becomes

$$(v \rightarrow) - (v \leftarrow) = 2\frac{k_b T}{h_p} \exp\left(-\frac{\Delta F}{RT}\right) \sinh\left(\frac{f\lambda}{2k_b T}\right) \tag{4}$$

This derivation in the context of studying shearing resistance of soils was originally conceived by Mitchell (1964). At any instant, the number of flow units that are successful in crossing the energy barrier is obtained by the multiplication of the total number of flow units and the frequency/probability as defined in equation (4).

In this context, soils are described as assemblies of particles in equilibrium, with forces sustained and transferred thorough solid-to-solid contacts between adjacent particles (Mitchell, 1964). From the perspective of an individual particle, movement is prevented by several inter-particle contacts between neighbours. Erosion of soil particles involves two processes, displacement and transport, of the individual particles. It is postulated that the former process requires relative movement primarily through sliding and/or rolling at inter-particle contacts, while the latter involves dilation of the soil structure when two adjacent particles must be pushed apart to create spaces for the displaced particles to move into. The postulated microstructural process is similar to that derived in explanation of soil deformation, shearing resistance and creep (Mitchell, 1964; Mitchell *et al.*, 1968, 1969). Although the engineering phenomena of soil deformation and shearing resistance are different from the internal erosion process in BEP by definition, the underlying mechanism might be entirely attributed to relative displacements and rearrangements of soil particles. This might be an explanation as to why these seemingly different processes have all been well described by the theory of rate processes. Further derivations of equations for computing erosion rate under hydraulic loading based on equation (4) are developed in the next section.

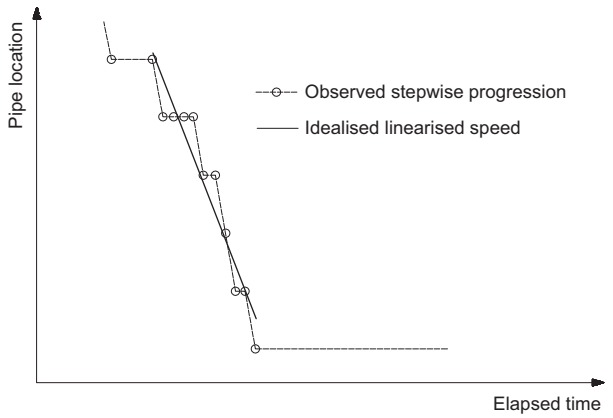

Fig. 2. Stepwise evolution of relative pipe location in a sand specimen with time in a laboratory erosion experiment (reproduced from data available in Robbins *et al.* (2018))

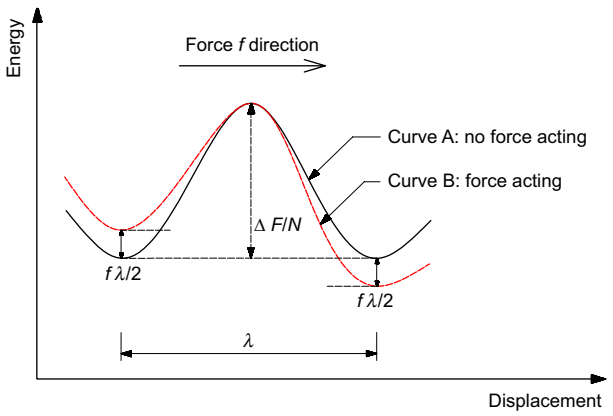

Fig. 3. Effect of a force on energy barriers (adapted from Mitchell & Soga (2005))

ANALYTICAL DERIVATION

In order to specialise the general rate process formulation presented above to the study of BEP, the concepts of energy

and power in the groundwater flow are first introduced in a porous cohesionless medium. Several researchers have proposed the application of a flow energy to represent the hydraulic loading that initiates and maintains the internal erosion of soil particles, as an alternative to traditional methods employing the hydraulic gradient and hydraulic shear stress as a metric for the description of erosion (Marot *et al*., 2012; Sibille *et al*., 2015; Kodieh *et al*., 2021; Gelet & Marot, 2022). Marot *et al*. (2012) developed an energy analysis on the internal erosion of cohesionless soils based on the energy conservation equation for the fluid phase. Details of this concept can be found in Marot *et al*. (2012), White (1999) and Sibille *et al*. (2015). Marot *et al*. (2012) proposed a measure of flow power to quantify the power carried by seepage flow which is expended for erosion. If a control volume of fluid flow is considered, through deductions based on the energy equations (White, 1999; Marot *et al*., 2012; Sibille *et al*., 2015), the flow power, P_{flow}, is given by

$$\begin{aligned} P_{\text{flow}} = &- \int_{S_\text{i}} (p\boldsymbol{v}\cdot\boldsymbol{n}_\text{i} + \gamma_\text{w} z\boldsymbol{v}\cdot\boldsymbol{n}_\text{i})\text{d}S \\ &- \int_{S_\text{o}} [(p+\Delta p)\boldsymbol{v}\cdot\boldsymbol{n}_\text{o} + \gamma_\text{w}(z+\Delta z)\boldsymbol{v}\cdot\boldsymbol{n}_\text{o}]\text{d}S \end{aligned} \tag{5}$$

where S_i and S_o are the inlet and outlet boundary surfaces of the control volume; p and $p+\Delta p$ are the static pressures at the inlet and outlet boundary surfaces; z and $z+\Delta z$ are the elevations at the inlet and outlet boundary surfaces; $\boldsymbol{v}$ is the flow velocity; $\boldsymbol{n}_\text{i}$ and $\boldsymbol{n}_\text{o}$ are, respectively, the outer unit normal vector of the inlet and the outlet boundary surfaces; and γ_w is the unit weight of water. There are five assumptions behind equation (5): (*a*) the energy is mainly dissipated by viscous shear at the direct vicinity of the solid particles; (*b*) the fluid temperature is constant; (*c*) the system is adiabatic; (*d*) a steady-state flow is considered; and (*e*) the flow is considered laminar (Marot *et al*., 2012; Gelet & Marot, 2022). The first assumption states that most of the energy expenditure in the flow is on dissipation during solid–fluid interactions, which directly contributes to erosion of soil particles. Sibille *et al*. (2015) demonstrated with results of laboratory internal erosion experiments that the energy expended on erosion may represent about 99% of the flow energy in all cases. However, in the case of surface erosion, this approximation may not hold with a turbulent fluid flow (Bagnold, 1980; Govers, 1992).

The instantaneous cumulative expended flow energy at time t can be calculated by integrating the instantaneous flow power over time:

$$E_{\text{flow}}(t) = \int_t^{t+\Delta t} P_{\text{flow}}\,\text{d}t \tag{6}$$

Based on the foregoing, one can define the volumetric flow energy and power densities as $\bar{P}_{\text{flow}}(t) = P_{\text{flow}}(t)/V$, and $\bar{E}_{\text{flow}}(t) = E_{\text{flow}}(t)/V$, respectively ($V$ is the control volume). Then, according to equation (6), $\bar{E}_{\text{flow}}(t) = \int_t^{t+\Delta t} \bar{P}_{\text{flow}}\,\text{d}t$.

Energy-based constitutive relationships have been demonstrated as an advantageous approach to evaluate the evolution of BEP in soil embankments (Kodieh *et al*., 2021). Therefore, in the present study, the authors formulate a new constitutive model based on the flow energy concept and the theory of rate processes to describe the evolution of BEP.

At any instant, the total number of flow units per unit volume times the probability of crossing energy barriers as defined by equation (4) gives the number of flow units eroded by hydraulic loading per unit volume per unit time:

$$\frac{\partial \bar{n}}{\text{d}t} = 2\bar{n}\frac{k_\text{b}T}{h_\text{p}}\exp\left(-\frac{\Delta F}{RT}\right)\sinh\left(\frac{f\lambda}{2k_\text{b}T}\right) \tag{7}$$

where $\bar{n}$ denotes the average number of flow units per unit volume. By virtue of the flow energy definition provided earlier, equation (7) can be rewritten as:

$$\frac{\partial \bar{n}}{\text{d}t} = 2\bar{n}\frac{k_\text{b}T}{h_\text{p}}\exp\left(-\frac{\Delta F}{RT}\right)\sinh\left(\frac{\bar{E}_{\text{flow}}V_\text{f}}{k_\text{b}T}\right) \tag{8}$$

where V_f is the idealised average volume of a flow unit, as defined by Andersland & Douglas (1970) and Gularte *et al*. (1980). In equation (8), the adjustment of the height of the free activation energy, as shown in Fig. 3, $f\lambda/2$ is replaced by $\bar{E}_{\text{flow}}V_\text{f}$, both referring to the energy expenditure on a given flow unit. Based on the aforementioned discussions, the flow energy density from the fluid flow $\bar{E}_{\text{flow}}$ can be estimated through integration of the flow power density $\bar{P}_{\text{flow}}$ over the unit time. Equations (7) and (8) are based on two assumptions on the control volume: (*a*) all flow units take part in erosion and are equally likely to be activated; and (*b*) flow energy is uniformly distributed over the control volume.

Let m_{fu} denote the average mass of a flow unit. By multiplying m_{fu} on both sides, equation (8) becomes

$$\frac{\partial \bar{n}}{\partial t}m_{\text{fu}} = 2\bar{n}m_{\text{fu}}\frac{k_\text{b}T}{h_\text{p}}\exp\left(-\frac{\Delta F}{RT}\right)\sinh\left(\frac{\bar{E}_{\text{flow}}V_\text{f}}{k_\text{b}T}\right) \tag{9}$$

The left-hand side of equation (9) represents the average mass erosion rate per unit volume, which is denoted as $\dot{m}$ in this paper:

$$\frac{\partial \bar{n}}{\partial t}m_{\text{fu}} = \dot{m} := \frac{\partial m}{\partial t}\frac{1}{V} \tag{10}$$

where $\partial m/\partial t$ gives the rate of erosion of soil mass (in units of mass over time).

The term $\bar{n}m_{\text{fu}}$ on the right-hand side of equation (9), representing the total mass of flow units per unit volume, is equal to the total mass of solid matter of soil particles per unit volume, which is usually defined as the dry bulk density of soil, ρ_{dry}.

Substituting $\dot{m}$ and ρ_{dry} into equation (9), one obtains:

$$\dot{m} = 2\rho_{\text{dry}}\frac{k_\text{b}T}{h_\text{p}}\exp\left(-\frac{\Delta F}{RT}\right)\sinh\left(\frac{\bar{E}_{\text{flow}}V_\text{f}}{k_\text{b}T}\right) \tag{11}$$

Mitchell *et al*. (1969) defined a parameter S as the idealised number of bonds per unit area, representing the number of inter-particle bonds averaged over a unit area, which is an important indicator of the soil structure. By assuming the separation distance between successive equilibrium positions as constant, the flow volume V_f can be expressed as

$$V_\text{f} = \frac{\lambda}{S} \tag{12}$$

where, according to Mitchell *et al*. (1969), a reasonable value of λ is assumed to be $2{\cdot}8 \times 10^{-10}$ m, which is the diameter of an oxygen ion. This assumption is based on the relatively constant surface structure of silicate layers on soil particles, both in clay and sand. By substituting equation (12) into equation (11), the following is obtained:

$$\dot{m} = 2\rho_{\text{dry}}\frac{k_\text{b}T}{h_\text{p}}\exp\left(-\frac{\Delta F}{RT}\right)\sinh\left(\frac{\bar{E}_{\text{flow}}\lambda}{Sk_\text{b}T}\right) \tag{13}$$

Equation (13) provides a constitutive relationship between the flow energy density and the erosion rate per unit volume, which follows a hyperbolic sine relationship. The dry bulk density, ρ_{dry}, and absolute temperature, T, can be measured from the soil sample, and k_b, R and h_p are known constants. Therefore, only two parameters need calibration to derive the

constitutive equation – namely, the activation energy, ΔF, and the number of flow units per unit area, S.

In the literature, the hyperbolic sine in equation (4) has often been approximated as an exponential (Mitchell, 1964; Mitchell *et al.*, 1969; Gularte *et al.*, 1980). Mitchell (1964) argued that, in the range of shearing stress of engineering interest, it suffices that $f\lambda/2kT > 1$ so that the hyperbolic sine can be approximated as exponential with reasonable accuracy. This approximation is well illustrated by the typical strain rate–shear stress curve at a given time after start of creep obtained from soil creep experiments as shown in Fig. 4(a). The cases when the shearing force f is too small to satisfy this condition were not considered. However, in the study of erosion, this kind of approximation cannot be adopted in equation (13), because when the flow energy is small and the approximation cannot be made, BEP may be initiating, making this portion of the curve very important (see Fig. 4(b)). Therefore, in this study, the hyperbolic sine in equation (13) is kept as per the mathematical derivations presented earlier:

$$\dot{m} = \alpha \sinh\left(\beta \bar{E}_{\text{flow}}\right) \tag{14}$$

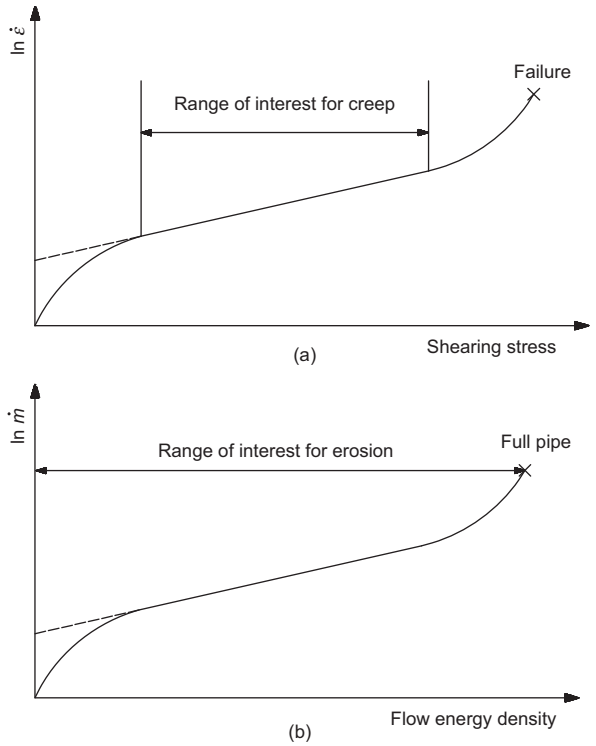

Fig. 4. Typical relationships between: (a) shearing stress and creep strain rate for a given time after start of creep; (b) flow energy density and mass erosion rate per unit volume

where the following substitutions were made for convenience:

$$\alpha = 2\rho_{\text{dry}} \frac{k_{\text{b}} T}{h_{\text{p}}} \exp\left(-\frac{\Delta F}{RT}\right) \tag{15}$$

and

$$\beta = \frac{\lambda}{S k_{\text{b}} T} \tag{16}$$

Equation (14) is a two-parameter relationship, which may be capable of describing the flow energy intensity–erosion rate characteristics of different soils. Under a given temperature, the parameter α is a function of the dry bulk density, ρ_{dry}, and the activation energy, ΔF, of the soil, the former of which can be easily measured. The parameter β is a function of the number of bonds per unit area, S. For a soil under study, several internal erosion tests are required to establish the values of α and β while maintaining a constant temperature and confining stress for all tests, through non-linear regression analysis of experimental data.

PRELIMINARY INVESTIGATION WITH EXPERIMENTAL OBSERVATIONS

The constitutive relationship derived in the previous section (see equation (14)) is first exercised to characterise quantitatively the values of free energy of activation ΔF and the number of bonds per unit area S from internal erosion experimental data provided in the literature. This comparison is used as a basis to evaluate the observed range of the two parameters, and shed light on the applicability of rate process theory to internal erosion mechanisms. Data from four different internal erosion tests with measurements of mass erosion rates are analysed. Specifically, Riha & Petrula (2023) performed BEP experiments on sand samples in a box with a 120 mm × 120 mm cross-section and a 350 mm erosion path. The testing apparatus and procedures employed in the suffusion experiments reported in the relevant references (Sterpi, 2003; Marot *et al.*, 2012; Sail *et al.*, 2011) are similar to cylindrical sand samples confined in rigid cells. The test parameters used in the study are summarised in Table 1. Detailed information on the tested materials is given in Table 2. The seepage direction is downward in the experiments conducted by Sail *et al.* (2011) and Marot *et al.* (2012), whereas an upward seepage direction in the experiment was reported by Sterpi (2003). Marot *et al.* (2012) carried out tests in a geotechnical centrifuge and different sample lengths were used. Constant vertical surcharge loads of 25 kPa and 14·2–42·5 kPa were applied during the experiments carried out by Sail *et al.* (2011) and Marot *et al.* (2012), respectively. In each experiment, prescribed hydraulic loading was applied to the specimens through hydraulic control components, while the eroded mass and flow rates were measured. The flow energy at any instant can

Table 1. Testing parameters of datasets reported in the literature

References	Type of test	Specimen dimensions: mm	Global hydraulic gradient	Vertical surcharge load: kPa	Centrifuge acceleration factor: g
Riha & Petrula (2023)	BEP	Box: 350(L) × 120 × 120	0·75–1·80	—	—
Sail *et al.* (2011)	Suffusion	Cylinder: 250–600 (H) × 280(D)	1–3	25	—
Sterpi (2003)	Suffusion	Cylinder: 140(H) × 70(D)	0·18–0·75	0	—
Marot *et al.* (2012)	Suffusion	Cylinder: 60–120(H) × 73(D)	45–150 (scaled)	14·2–42·5	13·3–40

Table 2. Description of tested materials

References	Components	Void ratio	Dry bulk density: g/cm^3	Particle size, D_{50}: mm	Uniformity coefficient, C_u	Gradation
Riha & Petrula (2023)	Three medium sands: grain size 0/2 mm	0·40–0·62	1·63–1·88	0·63–1·13	1·84–2·98	Uniform
Sail *et al.* (2011)	Mixture of glass beads: 40% small + 60% large	0·36	1·84	1·42	14·43	Gap graded
Sterpi (2003)	Recovered Milano natural sand	0·51	1·80	0·36	39·32	Well graded
Marot *et al.* (2012)	Clayey sand: 90% Fontainebleau sand + 10% kaolinite clay	0·42	1·91	0·20	2·49	Poorly graded

be computed from the applied hydraulic gradient and flow rate measurements from equations (5) and (6). Temperatures were not reported or controlled in these experiments. Since temperature plays an important role in the theory of rate processes, the results of experiments and the analysis below could be affected if temperatures were controlled during the experiments.

The parameters α and β in equation (14) are estimated through non-linear regression on the experimental data (Teunissen, 1990). Fig. 5 reports the topology of the objective function (i.e. the residual sum of squares (RSS) on the observations) from one dataset for the non-linear regression analysis carried out. For each case, two local minima are detected from the 3D plots and are labelled as 'local min #1' and 'local min #2', respectively. Therefore, as shown in Fig. 6, on each dataset, two separate non-linear least-squares regressions were performed with initial values of α and β corresponding to the two local minima to obtain accurate estimates of α and β. A 95% confidence interval was plotted together with each non-linear regression curve. Non-linear regression NL1 (corresponding to local min #1) predicts that the erosion rate accelerates at lower flow energy densities (when $\bar{E}_{\text{flow}} > 25\,\text{J/m}^3$ for Riha & Petrula (2023), $\bar{E}_{\text{flow}} > 3\,\text{J/m}^3$ for Sail *et al.* (2011) and $\bar{E}_{\text{flow}} > 0{\cdot}1\,\text{J/m}^3$ for Sterpi (2003) and Marot *et al.* (2012)), whereas non-linear regression NL2 (corresponding to local minimum #2) predicts that acceleration in erosion rate occurs at higher flow energy levels outside the range observed in the experiments. The dataset from Riha & Petrula (2023) contains a much larger amount of data and covers a wider range of flow energy densities, up to 40 J/m^3. Interestingly, the erosion rates predicted by the two regression curves on the data from Riha & Petrula (2023) (Fig. 6(a)) show a much more consistent trend (with respect to each other) when compared to the other selected internal erosion tests. Moreover, in the observations of Marot *et al.* (2012), there is no evidence that the erosion rate is accelerating, unlike Sail *et al.* (2011) and Sterpi (2003); this difference is especially obvious in the data from Sterpi (2003) as the flow energy density magnitudes are similar to Marot *et al.* (2012). The higher-valued datapoints in the small flow energy density regime are very well captured with the NL2 parameters for Sterpi (2003) and Marot *et al.* (2012) datasets. At higher flow energy density values ($> 0{\cdot}15$ J/m^3), the two experiments appear to differ in their behaviour; Sterpi (2003) shows acceleration in mass loss and Marot *et al.* (2012) does not. For regression with the BEP data in Riha & Petrula (2023), the 95% confidence interval of NL2 is narrower than that of NL1 at higher flow energy density, indicating a higher plausibility of NL2 in this case. For suffusion data from Sail *et al.* (2011) and Sterpi (2003), the 95% confidence intervals of NL1 are narrower than those of NL2, while for the data from Marot *et al.* (2012) the interval widths of two regressions are similar. With the regression analysis, it is not possible to conclude which of the two regressions is more

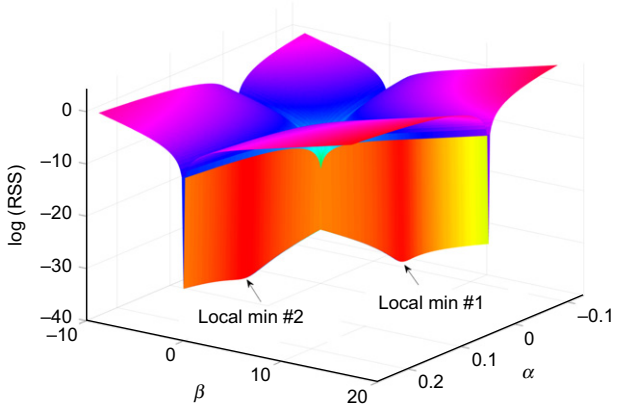

Fig. 5. Topology of RSS from regression analysis on data available in Marot *et al.* (2012), RSS at local min #1: $2{\cdot}5 \times 10^{-33}$, RSS at local min #2: $1{\cdot}3 \times 10^{-33}$

representative of the true behaviour of the soil for prediction purposes. Notwithstanding the significant differences between the reported tests, both in terms of testing conditions and materials, the results demonstrate that the estimated values of ΔF and S fall within a consistent range, highlighting how the theory of rate processes can describe internal erosion mechanisms. The results obtained, in terms of activation energy and number of bonds, represent the basis for the BEP investigations proposed in the following.

Activation energy measures

The calculated activation energy values, along with those reported in the literature, are summarised in Table 3. The values for the activation energy from the selected datasets are 96·9–134·6 kJ/mol and 74·9–97·0 kJ/mol as estimated from NL1 and NL2, respectively. Values from both regressions fall into the range of measurements from creep and surface erosion experiments reported in the literature (Mitchell *et al.*, 1969; Andersland & Douglas, 1970; Christensen & Das, 1973; Gularte *et al.*, 1980; Murayama *et al.*, 1984). The estimated activation energy values from NL1 in this study are close to those reported for creep (Mitchell *et al.*, 1969; Andersland & Douglas, 1970; Murayama *et al.*, 1984), and are higher than those reported from surface and hole erosion tests (Christensen & Das, 1973; Gularte *et al.*, 1980). In contrast, the activation values from NL2 on the internal erosion data are closer to those from surface erosion tests and lower than creep.

According to the discussions above, activation energy ΔF represents the energy expenditure to activate one mole of flow unit. Mitchell & Soga (2005) hypothesised that movement of each soil particle requires rupture of single solid-to-solid bonds or simultaneous rupture of several such bonds between soil particles at contact. Physical evidence for the presence of

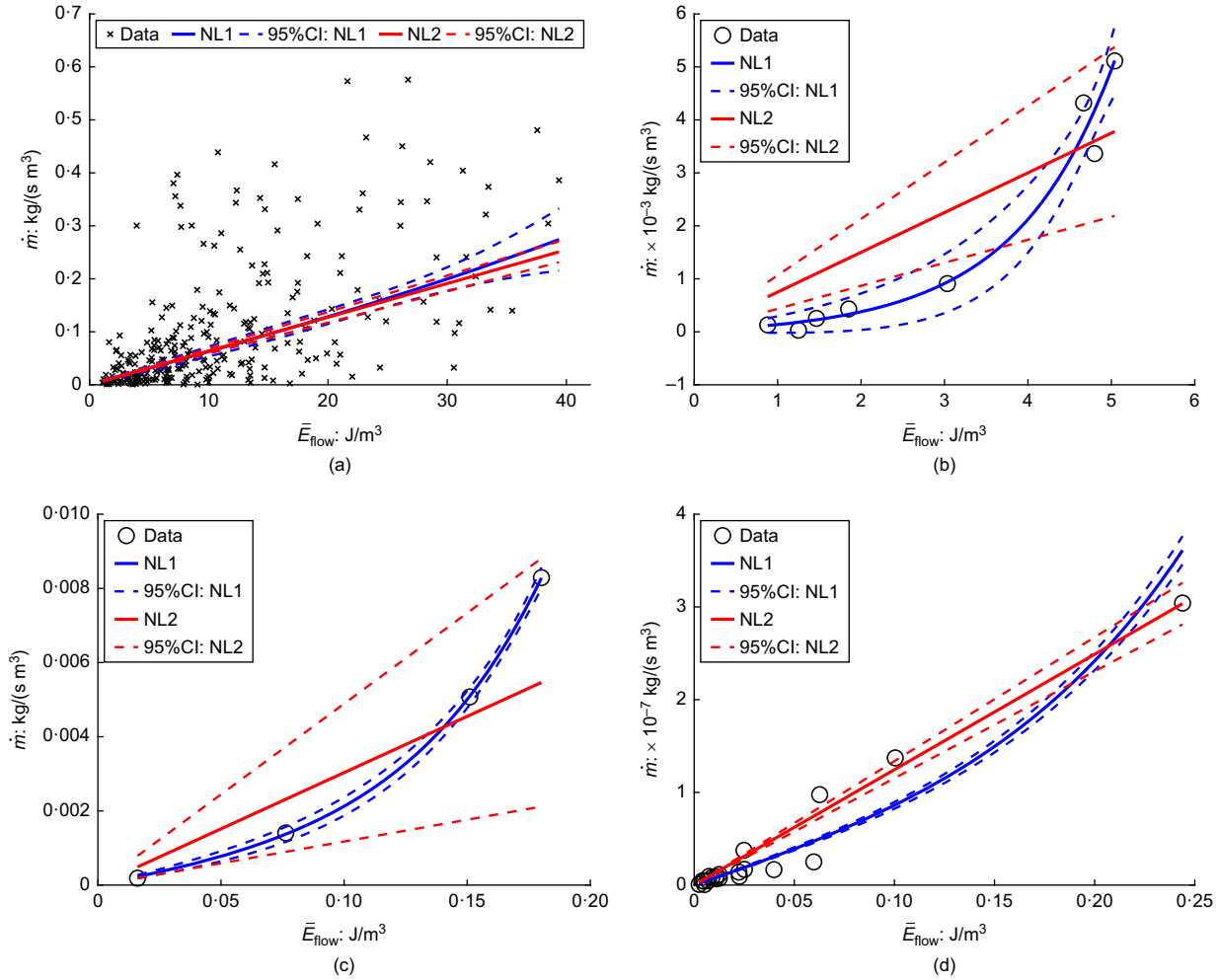

Fig. 6. Non-linear regression on data obtained from: (a) BEP experiments in Riha & Petrula (2023), and suffusion experiments in (b) Sail *et al.* (2011), (c) Sterpi (2003) and (d) Marot *et al.* (2012)

Table 3. Values of activation energy estimated from various studies

Material	Type of test	Activation energy: kJ/mol	References
Medium sand	Internal erosion, BEP	96·9*/79·1†	Present study (data based on Riha & Petrula (2023))
Mixed glass beads	Internal erosion, suffusion	116·0*/77·1†	Present study (data based on Sail *et al.* (2011))
Milano sand	Internal erosion, suffusion	111·6*/74·9†	Present study (data based on Sterpi (2003))
Clayey sand	Internal erosion, suffusion	134·6*/97·0†	Present study (data based on Marot *et al.* (2012))
Grundite, remoulded	Surface erosion	72·8–107·0	Gularte *et al.* (1980)
Grundite	Hole erosion	64·5	Christensen & Das (1973)
Kaolinite	Hole erosion	68·2	Christensen & Das (1973)
Sault St Marie clay	Creep	117	Andersland & Douglas (1970)
Osaka clay, normally consolidated	Creep	120–134	Murayama & Shibata (1961)
Illite, remoulded	Creep	105–165	Mitchell *et al.* (1969)
Illite, dry	Creep	155	Mitchell *et al.* (1969)
San Francisco Bay mud, undisturbed	Creep	105–135	Mitchell *et al.* (1969)
Sacramento River sand, dry	Creep	105	Mitchell *et al.* (1969)

*Estimated from regression NL1.
†Estimated from regression NL2.

solid-to-solid contacts and inter-particle bonds has been obtained in both clays and sands (Matsui *et al.*, 1980; Albalasmeh & Ghezzehei, 2014). Furthermore, Mitchell & Soga (2005) proposed that the cause of creep movements of soil particles and rupture of inter-particle bonds is the slow diffusion of oxygen ions in and around inter-particle

contacts. This interpretation accounts for the features of the estimated values of the activation energy from previously reported results: (*a*) the activation energy values fall into the range of chemical reactions (40–400 kJ/mol) (*b*) the magnitude of the activation energy does not vary much with changes in water content, consolidation pressure and void ratio; and (*c*) the values of activation energy are similar for both sands and clays. This postulate is consistent with the fact that the calculated values of activation energy from this study are of similar magnitudes themselves and fall within the range of previously reported estimates, even though the type of experiments and soils are significantly different than the previously described research.

Number of bonds per unit area

Table 4 reports the estimated number of bonds per unit area, along with those reported in the literature. The values estimated herein are $0{\cdot}41 \times 10^{10}$–$3{\cdot}25 \times 10^{12}$ and $0{\cdot}42$–$7{\cdot}81 \times 10^{16}$ from NL1 and NL2, respectively. The values from NL1 are slightly larger than those estimated from surface erosion tests (Christensen & Das, 1973; Gularte *et al*., 1980), four to five orders of magnitude smaller than those reported for creep by Mitchell *et al*. (1969), and about ten orders of magnitude smaller than that of Andersland & Douglas (1970) for creep. The computed numbers of bonds per unit area in this study with NL2, however, are six orders of magnitude larger than those from NL1.

Mitchell *et al*. (1969) studied the relationships between the number of bonds per area, effective stress and strength of different soils. From their study, the number of bonds is shown to be proportional to the magnitude of the effective stress, and the strength of a soil is found to be directly proportional to the number of these bonds. The same proportionality between the number of bonds and the soil strength holds for both clay and sand. Furthermore, Mitchell *et al*. (1969) showed that, at any value of effective stress, the number of bonds per area is about the same for sand and clay, independent of particle size. A plausible physical interpretation for these experimental results is proposed by Mitchell & Soga (2005), stating that the bonds are possibly of the primary valence type formed between oxygen atoms and silicon atoms at inter-particle contacts that transmit the effective stress. Mitchell & Soga (2005) further assumed that the number of bonds formed at a single contact is proportional to the effective stress transmitted through the contact. Michalowski *et al*. (2018) characterised the surface texture of silica sand grains and visualised inter-granular contacts composed of many microscopic 'contact points' with scanning electron microscopy (SEM). Wang (2017) demonstrated force transmission mechanisms at inter-granular contacts through microscopic contact points with discrete-element modelling (DEM).

Remark. The erosion model under investigation was developed from fundamental granular physics in the context of simulating BEP through the theory of rate processes, which has been proven capable of describing various processes in sands, such as surface and hole erosion. The main reason why both BEP and suffusion test data are included in this section is to show that the activation energy and number of bonds estimated through the model provide values that are reasonably similar for both cases and fall into the ranges reported in the literature. This is an interesting finding, because it opens up possibilities for a more fundamental understanding of internal erosion phenomena, based on the microgranular effects described through the theory of rate processes. At the same time, the authors remark that the proposed model was developed to describe BEP; therefore, no claim is made as to its capability of simulating suffusion. However, the authors believe that the fundamental description of internal erosion mechanisms as rate processes could be of value to other research groups that might use the theoretical framework developed herein and extend it to suffusion (based on the observation that the estimated parameters fall within a narrow range).

NUMERICAL INVESTIGATIONS ON BEP PROGRESSION

The constitutive relationship proposed in this study is evaluated by incorporating it into a multiphase numerical model. Numerical simulations of temporal BEP progression are conducted within this framework, and the results are compared with experimental findings obtained from the literature, to serve as calibration and validation. In particular, the calibrated values of activation energy and number of bonds are compared with those estimated from the regression analysis presented in the previous section and the values

Table 4. Values of number of bonds per unit area from various studies

Material	Type of test	Number of bonds per unit area: m^{-2}	References
Medium sand	Internal erosion, BEP	$3{\cdot}25 \times 10^{12}$ */$0{\cdot}42 \times 10^{16}$ †	Present study (data based on Riha & Petrula (2023))
Mixed glass beads	Internal erosion, suffusion	$8{\cdot}01 \times 10^{10}$ */$7{\cdot}81 \times 10^{16}$ †	Present study (data based on Sail *et al*. (2011))
Milano sand	Internal erosion, suffusion	$0{\cdot}41 \times 10^{10}$ */$0{\cdot}45 \times 10^{16}$ †	Present study (data based on Sterpi (2003))
Clayey sand	Internal erosion, suffusion	$0{\cdot}77 \times 10^{10}$ */$1{\cdot}66 \times 10^{16}$ †	Present study (data based on Marot *et al*. (2012))
Grundite, remoulded	Surface erosion	$0{\cdot}46$–$1{\cdot}82 \times 10^{9}$	Gularte *et al*. (1980)
Grundite	Hole erosion	$3{\cdot}45 \times 10^{9}$	Christensen & Das (1973)
Kaolinite	Hole erosion	$5{\cdot}75 \times 10^{9}$	Christensen & Das (1973)
Sault St Marie clay	Creep	$1{\cdot}65 \times 10^{20}$	Andersland & Douglas (1970)
Illite, remoulded	Creep	3–20×10^{14}	Mitchell *et al*. (1969)
Illite, dry	Creep	5×10^{16}	Mitchell *et al*. (1969)
San Francisco Bay mud, undisturbed	Creep	2–10×10^{14}	Mitchell *et al*. (1969)
Atioch sand, dry	Creep	4–20×10^{14}	Mitchell *et al*. (1969)

*Estimated from regression NL1.
†Estimated from regression NL2.

reported for surface erosion, hole erosion and creep in the literature. Sensitivity analysis is performed on different modelling parameters to study their influence on the simulation results.

Model implementation

As originally presented in Fascetti & Oskay (2019a), the groundwater flow during the erosion process in the embankment is idealised using a non-linear diffusion equation:

$$\frac{\partial h(x,t)}{\partial t} = \nabla \cdot [D(x,t)]\nabla h(x,t) \quad x \in \Omega,\ t \in (0,T) \tag{17}$$

where $h(x, t)$ represents the hydraulic head field; Ω is the computational domain; T is the total time; and $D(x, t)$ is the diffusivity coefficient of the soil:

$$D(x,t) = \frac{k(x,t)}{S_s} \tag{18}$$

where $k(x, t)$ is the soil conductivity and S_s is the specific storage of the soil.

The computational domain is subject to the following boundary conditions:

$$h = h_b(t) \text{ on } \Gamma_b \subset \partial\Omega \tag{19}$$

$$q \equiv -D\frac{\partial h}{\partial x} = q_b \text{ on } \Gamma_q \subset \partial\Omega \tag{20}$$

with $\Gamma_b \cap \Gamma_q = \varnothing$. q is the outward flux; q_b is the prescribed boundary flux; and h_b is the time-dependent prescribed hydraulic head at the boundary.

The mass balance equation for the fluidised particles reads:

$$\frac{\partial[\gamma(x,t)\phi(x,t)]}{\partial t} + \frac{\partial(\gamma(x,t)q(x,t))}{\partial x} = \frac{\partial\phi(x,t)}{\partial t} \tag{21}$$

where $\gamma(x, t)$ is the concentration of soil particles fluidised by the erosion process (i.e. the ratio between the volume of fluidised particles and the total volume of the fluid); and $\phi(x, t)$ is the soil porosity. It is worth mentioning that a limit porosity criterion is enforced in the simulations to guarantee numerical stability. Such a value represents the maximum local porosity attained for fully piped conditions (i.e. $\phi(x, t) \leq \phi_{lim}$, with ϕ_{lim} being a model parameter). Based on its definition, such limit porosity is inherently different from the average maximum porosity measured from standard testing procedures (e.g. ASTM, 2016), which represents the average porosity of a soil sample in its loosest condition.

Recalling equation (10), the right-hand side of equation (21) can be written as

$$\frac{\partial\phi(x,t)}{\partial t} = \frac{\dot{m}}{\rho_s} \tag{22}$$

where ρ_s is the density of soil particles. By substituting the constitutive relationship given in equation (14) into equation (22):

$$\frac{\partial\phi(x,t)}{\partial t} = \frac{1}{\rho_s}\alpha \sinh\left[\beta\bar{E}_{flow}(x,t)\right] \tag{23}$$

With the governing equations introduced above, a typical one-dimensional (1D) erosion problem was simulated. To solve the system of equations, the response field is discretised along the 1D domain represented by the erosion path. Discretisation in space is performed by means of a central finite-difference scheme, while time is discretised by means of the Crank–Nicolson algorithm. The modelling procedure is as follows.

(*a*) Define and discretise the computational domain; assign initial values for the modelling parameters and boundary conditions. A higher local hydraulic gradient arises at the downstream exit area.
(*b*) At every time increment, the hydraulic head in the domain is computed through equation (17), and the hydraulic gradient is calculated. Compute flux with Darcy's law and porosity evolution rate with the constitutive relationship equation (23), with the computed hydraulic gradient and the conductivity. In practice, a threshold gradient value is often observed below which soil mass erosion either does not initiate or mass loss is too small to cause a change in porosity (e.g. Robbins *et al*. (2018)). In these cases, a threshold gradient is used to calculate a cut-off flow energy density, which is subtracted from the flow energy density values used in the computation.
(*c*) Compute the concentration of fluidised particles from the mass balance equation (21); update conductivity using the Kozeny–Carman equation; and update diffusivity. The simulation continues until the target total time or number of iterations is met. In a case where the initial state provided in step (*a*) does not introduce a local gradient that exceeds the critical value, the solution is trivial and piping does not progress through the domain.

Experimental works simulated

The multiphase numerical framework described above is used to simulate the BEP experiments reported in Robbins *et al*. (2018), Vandenboer *et al*. (2019) and Pol *et al*. (2022). In the BEP experiment performed by Robbins *et al*. (2018), a sand sample with a 958 mm erosion path was tested in an acrylic cylinder with an internal diameter of 76·2 mm, with a free slope exit condition at the downstream end. In Vandenboer *et al*. (2019) and Pol *et al*. (2022), sand samples were tested in boxes with lengths of erosion path of 352 mm and 300 mm, respectively, a width of 300 mm and a height of 100 mm; the samples were covered by an acrylic lid with an exit hole downstream. In these experiments, the progression rates of piping were monitored through time-stamped video data, and local hydraulic heads were measured during the tests using pressure gauges installed along the erosion paths. While the set-ups of the experiments from Robbins *et al*. (2018) and Pol *et al*. (2022) were designed to produce a 1D erosion path for convenient gradient measurements, the test set-up in Vandenboer *et al*. (2019) was designed to resemble more realistic 3D conditions.

Simulation results

The model parameters used in all the reported simulations are summarised in Table 5. The values of activation energy and the number of bonds estimated from the regression analyses presented in the previous section were employed as initial values for the calibration. Based on the discussion and theoretical derivations, activation energy is viewed as an intrinsic property of soils, and therefore its value was calibrated from the experiment performed by Robbins *et al*. (2018) and maintained constant in all the other simulations. The threshold gradients used for the calculations are the same as the global average gradients. This choice was made to provide consistency with the reported experimental results, which also include information on global gradients. The limit porosity values were also calibrated from the experimental data. The limit porosity value that was calibrated from data

Table 5. Calibration of model parameters in 1D erosion simulation with data obtained from: R-test 7B in Robbins *et al.* (2018), V-test with gradual loading in Vandenboer *et al.* (2019) and P-test FPH_237 in Pol *et al.* (2022)

Parameter	*R*	*P*	*V*
Length of erosion path: mm	958	352	300
Global and threshold gradient	0·41	0·19	0·20
Initial porosity	0·379	0·399	0·403
Hydraulic conductivity: 10^{-4} m/s	6·20	1·10	1·03
Limit porosity	0·624*	0·549*	0·549
Specific storage: 10^{-5} m^{-1}	7·20*	7·57	7·64
Activation energy, ΔF: kJ/mol	73·70*	73·70	73·70
Number of bonds, S: 10^{13} m^{-2}	6·76*	9·92*	12·65*

*Calibrated with experimental results.

in Pol *et al.* (2022) was employed in the simulation for the test from Vandenboer *et al.* (2019), since the soils tested in these experiments were similar. Similarly, the value of specific storage in the simulation of the experiment from Robbins *et al.* (2018) was first calibrated. Based on the calibrated specific storage value, the power law relationship proposed by Kuang *et al.* (2020) was employed to evaluate specific storage values in the simulations of the tests reported by Vandenboer *et al.* (2019) and Pol *et al.* (2022). As illustrated by Table 5, the values of the number of bonds per unit area S calibrated with observations from independent BEP experiments with different sands fall into the range of values reported in the literature for various mechanisms (see Table 4). These results further demonstrate the capability of the proposed constitutive model to describe BEP at a fundamental level.

Figure 7 reports the comparison of the simulation results with the experimental observations from Robbins *et al.* (2018) in terms of pipe progression rate (Fig. 7(a)) and the evolution of local hydraulic gradients (Fig. 7(b)). The comparison between numerical and experimental pipe progression rates was employed as a means to calibrate the model parameters, as reported in Table 5. A satisfactory agreement is achieved in the average pipe progression rate and both numerical and experimental curves exhibit a relatively constant progression rate during the whole process. It is worth noting that in the comparison the experimental curve was shifted by 70 mm to account for the difference in identification of the pipe tip in the experiments, when compared to the numerical results. A significant difference between the experimental and simulation outcomes that can be observed in Fig. 7(a) is in the step size of pipe progression; the pipe progressed in non-uniform steps during the experiment, but in uniform and smaller steps in the simulation. Two idealisations in the simulation might have contributed to this behaviour: (*a*) the time resolution is much higher in the numerical simulation than the measurement frequency in the experiment; (*b*) the diffusion equation, equation (17), might smooth out the local spatial heterogeneities of seepage flow, which are inherently present in the experiments (Powell & Richerson, 1985).

Figure 7(b) shows the comparison of the evolution of local hydraulic gradients during the experiment, demonstrating an excellent agreement. It is worth highlighting that the simulation with model parameters calibrated using the pipe progression rate successfully reproduced the evolution of local gradients observed in the experiment. This cross-validation from two independent features observed in the experiment provides supporting evidence for the validity of the proposed approach. The observed local gradients further dropped to the range of 0·10–0·25 after the pipe tip passed

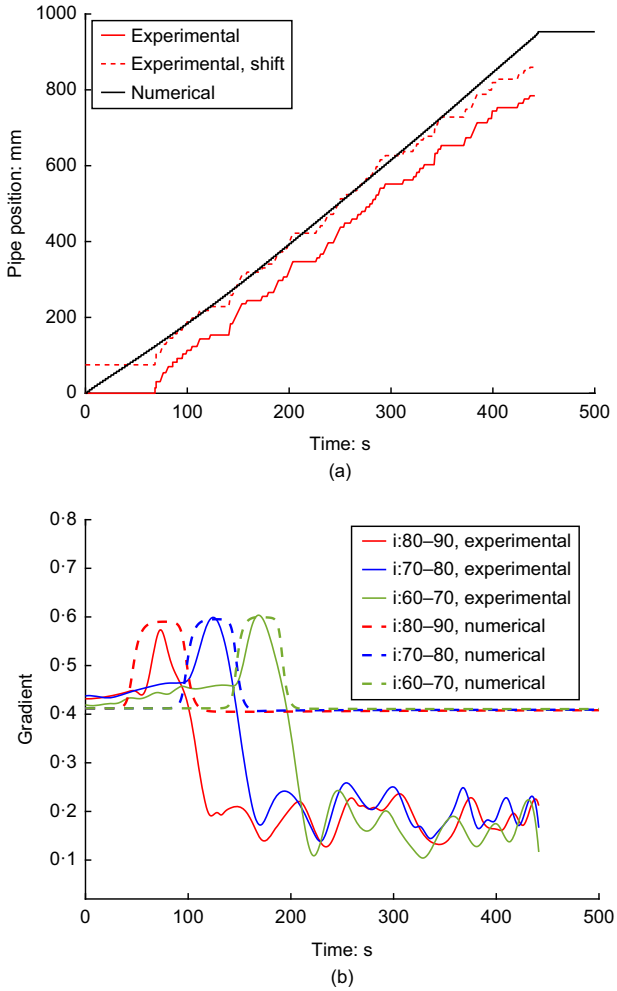

Fig. 7. Comparisons of simulation results and experimental data: (a) pipe progression rate; (b) evolution of local gradients (experimental data available in Robbins *et al.* (2018))

through, while the simulation results show that the local gradients fell back to the initial value of 0·41 after the passage of the pipe. One possible explanation for this discrepancy is that, during the experiment, once the pipe had progressed entirely through the sample, the upstream hydraulic head was no longer maintained constant, causing a decrease in the value of the head at the upstream side and consequently in the hydraulic gradient. Conversely, the upstream and downstream hydraulic heads were maintained constant throughout the simulation. Since the further drops in gradients were also observed in other experimental works (e.g. in Pol *et al.* (2022)), another explanation is that the resistance to seepage flow in the pipe is much lower than in the soil. Moreover, a sudden step forward in pipe progression, as observed in the experiment, might have contributed to the different heights between the first gradient peaks in the experimental and numerical data in Fig. 7(b). By a closer look at both Figs 7(a) and 7(b), the first gradient peak happened at about 70 s when the pipe location experienced a sudden step forward. Robbins *et al.* (2018) pointed out that when pipe progressed rapidly through the sample, the hydraulic conditions were likely not to be near equilibrium, which might be the reason for the lower height of the first peak in the gradient. In contrast, during the simulation, the hydraulic equilibrium of the model was ensured by choosing a stable computational time step when applying the Crank–Nicolson method (Thomas, 2013; Fascetti & Oskay, 2019a). Overall, the good agreement on both pipe progression rates

and the evolution of local gradients demonstrates the capability of the multiphase model in capturing the main hydraulic conditions in the soil during BEP progression.

Figures 8–10 illustrate calibration and validation of the model with data from BEP experiments performed by Vandenboer *et al.* (2019) and Pol *et al.* (2022). The model parameters for the test in Pol *et al.* (2022) were calibrated with the pipe progression rate measured from test FPH_237, with a global hydraulic gradient of 0·19 and an average pipe progression rate of 0·064 mm/s. As shown in Figs. 8 and 9, the model is capable of replicating the experimental pipe progression curves. Once the model parameters were calibrated, four other experiments with two types of different sands and different hydraulic conductivity values were employed for validation, as shown in Fig. 10. The increasing trend of pipe progression rate with increasing hydraulic conductivity, which was demonstrated in Pol *et al.* (2022), is well captured by the model. Discrepancies exist between the validation data points with hydraulic conductivity values of 0·26 mm/s and 1·00 mm/s, for which the measured progression rates are lower than those predicted by the simulations. This difference could be ascribed to the variability in testing conditions and soil properties within the samples in the various experiments, as BEP has been demonstrated to be highly sensitive to spatial variation in soil properties by Negrinelli *et al.* (2016).

Sensitivity analysis

A sensitivity analysis was performed to assess the effect of the different model parameters on the simulation results. In particular, the sensitivity to the meshing resolution, coefficients of the hyperbolic sine constitutive law, initial diffusivity, and limit porosity of the sand specimen was investigated. A one-at-a-time method was employed for the sensitivity analysis, which analyses the effect of one parameter on simulation results at a time while keeping the others fixed (Saltelli *et al.*, 2008). The outcome of simulations with different mesh densities is given in Fig. 11. The simulation results of the general trend of pipe progression were not affected by the mesh density, except for a variation in the step sizes of pipe propagation, which derives from the different spatial resolution. Therefore, when step sizes are not a concern, a high mesh density is not necessary to save simulation time and computational resources. The sensitivity of the simulation results to the coefficients of the hyperbolic sine constitutive law, initial diffusivity and limit porosity of the sand specimen is summarised in Fig. 12. The sensitivity is illustrated as the variation of the normalised average velocity of pipe progression with respect to changes of the model parameters under exam. The normalised average velocity of pipe progression is defined as the average velocity of pipe progression, which is equal to the sample length divided by time for the formation of a full pipe, divided by the average

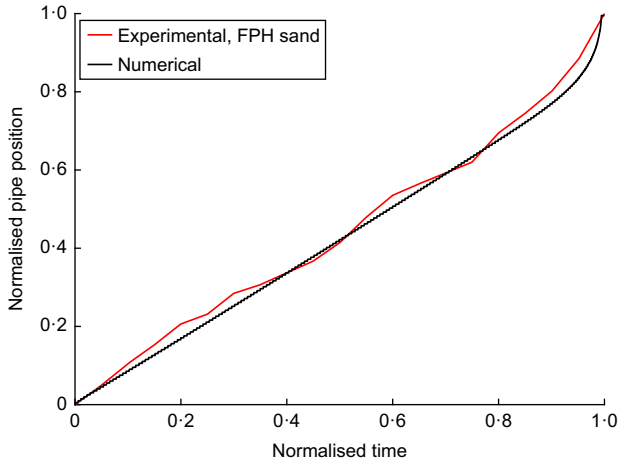

Fig. 8. Calibration of model with BEP experimental data from test FPH_237 in Pol *et al.* (2022)

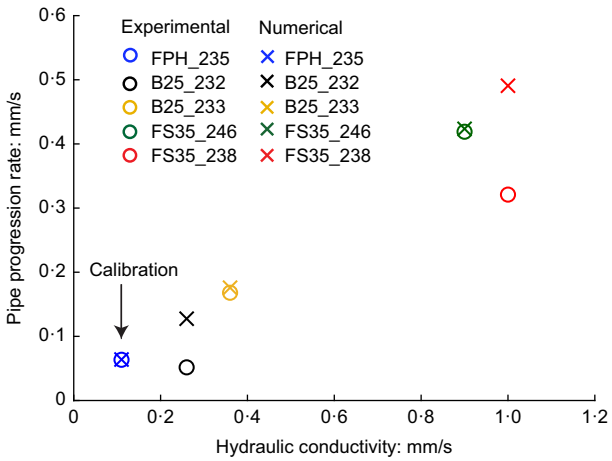

Fig. 10. Validation of simulation results with data from BEP experiments (data in Pol *et al.* (2022))

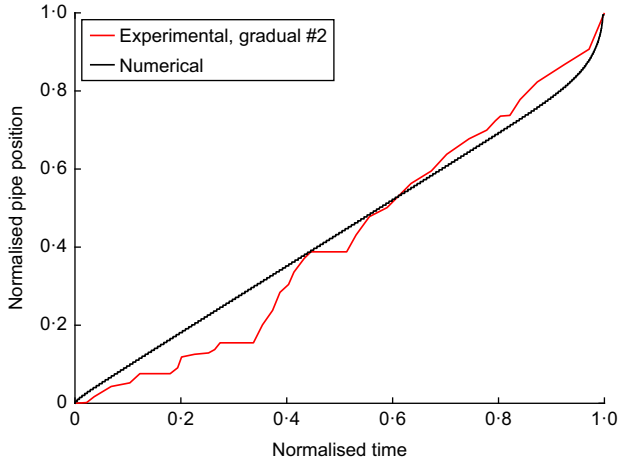

Fig. 9. Calibration of model with BEP experimental data from test gradual#2 in Vandenboer *et al.* (2019)

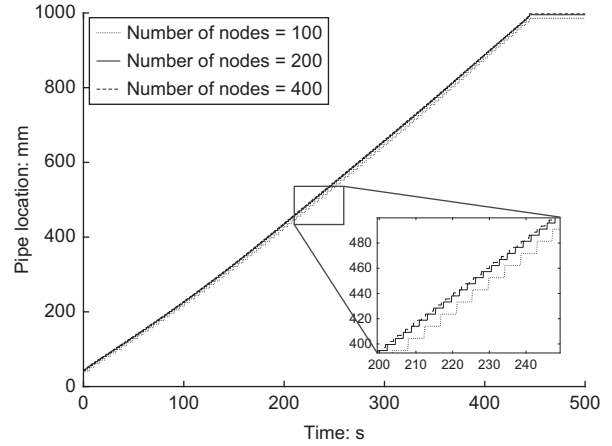

Fig. 11. Influence of the meshing resolution on the simulated pipe progression

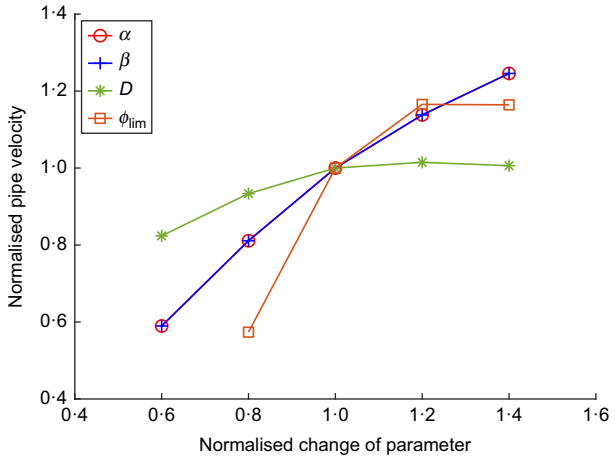

Fig. 12. Influence of the model parameters on the simulated time to development of full pipe

velocity of pipe progression computed with the original parameters in Table 5. As shown in Fig. 12, the pipe progression speeds up with increase of all the four parameters under study. For smaller parameter values (i.e. normalised values smaller than 1), the simulation results are more sensitive to the limit porosity, followed by the hyperbolic sine coefficients, and are the least sensitive to the initial diffusivity. For larger parameter values (i.e. normalised values larger than 1), the sensitivity of the model to both the initial diffusivity and the limit porosity decreases, while the sensitivity to the two hyperbolic sine coefficients is generally higher, as expected. In the range of variation considered herein (0·6–1·4), the effects of changes in the two hyperbolic sine coefficients are similar, and the velocity of pipe progression changes approximately in a linear fashion with changes in each of these two parameters.

DISCUSSION ON SIMULATION RESULTS

The model parameters ΔF and S calibrated from the comparisons with the BEP experimental results are equal to 73·70 kJ/mol and $6{\cdot}76–12{\cdot}65 \times 10^{13}$ m^{-2}, respectively. Referring to the values listed in Tables 3 and 4, the estimated activation energy values and numbers of bonds per unit area from NL2 are more plausible according to the following reasoning: (*a*) estimated values of activation energy are in good agreement with those calibrated from the simulations, as hypothesised during model development; (*b*) the values for the number of bonds calibrated from the simulations are consistent with those obtained from NL2, by taking into account the influence of the effective stress in the soil in Mitchell *et al.* (1969), as the sand specimens in Robbins *et al.* (2018), Vandenboer *et al.* (2019) and Pol *et al.* (2022) were tested without applying surcharge loads. Moreover, during the experiments progressive pipes were visualised in the samples, which means, according to Fleshman & Rice (2014), a loosened zone being present in the vicinity of the pipe tip. Fleshman & Rice (2014) have shown that this loosened zone has a greater porosity and, therefore, a smaller average effective stress. In addition, the samples in Sail *et al.* (2011) and Marot *et al.* (2012) were tested under surcharge loads of 14–43 kPa, which yielded greater effective stresses in the samples, as discussed earlier. Therefore, it is likely that the average effective stresses in the loosened zone in the soil samples in the BEP experiments were smaller than those in the samples of the other suffusion experiments, but at the same time can be expected to be larger than that of the hole and surface erosion tests reported in Christensen & Das (1973) and Gularte *et al.* (1980), in which soil particles were eroded from a free surface. Consequently, it is reasonable that the values of number of bonds per unit area calibrated from the simulations ($6{\cdot}76–12{\cdot}65 \times 10^{13}$ m^{-2}) fall between those from the suffusion tests ($\sim 10^{15}$ to 10^{16}) and surface/hole erosion tests ($\sim 10^{9}$). The number of bonds per unit area estimated from data available in Sterpi (2003) is smaller than those from the other two datasets. This is likely to be accounted for by the same reasoning, since the samples in this set of tests were not loaded.

Comparing the calibrated values of activation energy and numbers of bonds per area with those reported for surface erosion, hole erosion and creep in the literature (refer to Tables 3–5), variations may be explained based on the proposed constitutive model. Should the postulates of Mitchell *et al.* (1969) and Mitchell & Soga (2005) on activation energy and number of bonds per unit area be accepted, values of activation energy would not vary significantly with either types of soil or testing conditions, and numbers of bonds per unit area should remain proportional to the effective stresses. The calibrated value of activation energy from the BEP datasets (73·7 kJ/mol) falls into the range of those from surface/hole erosion tests (65–107 kJ/mol), but is significantly lower than those from creep tests (105–165 kJ/mol). Christensen & Das (1973) explained this discrepancy in activation energy values in two ways. First, inaccuracies in temperature control and crude measurements during the tests cannot be excluded. Second, data from erosion tests cannot be obtained until failure conditions are imminent, thus the activation energy computed from the erosion tests pertains to near-failure conditions. Moreover, Mitchell *et al.* (1968) observed that estimated activation energy decreases as failure conditions approach. The calibrated values of number of bonds per unit area based on the BEP datasets ($6{\cdot}76–12{\cdot}65 \times 10^{13}$ m^{-2}) are comparable to the estimates from creep tests of saturated soils ($\sim 10^{14}$) by Mitchell *et al.* (1969) and about three orders of magnitudes larger than those from surface and hole erosion tests ($\sim 10^{9}$). This can be attributed to the concentrated seepage pressure under which the local effective stresses in the erosion zones were comparable with those in soils in the creep tests and much larger than the local effective stresses in the soil during surface and hole erosion tests.

CONCLUSIONS

Based on fundamental granular physics, a constitutive model is proposed based on the theory of rate processes to describe BEP progression in GFPI systems. The theory of rate processes has been successfully used in studies of creep, surface and hole erosion of soils, but its applicability to BEP has not been explored previously. In the derivation of the constitutive model, the concept of flow energy density was adopted, as an alternative to more commonly used hydraulic gradient or hydraulic shear stress measures, because of its capability of better capturing both the initiation and progression phases during BEP, as previously demonstrated in the literature.

The proposed constitutive model was first exercised to perform regression analysis on available experimental data. The values of activation energy and number of bonds per unit area estimated from the experimental data align with the range of values reported in the literature for different processes in soils, and this consistency supports previous findings on the applicability of the rate of process theory to internal erosion mechanisms. In particular, both BEP and suffusion test data show that the activation energy estimated through the proposed model provides consistent values for the two different internal erosion mechanisms. This is an interesting finding, because it might lead to a more fundamental understanding of internal erosion phenomena, based on the microgranular effects described through the rate process theory.

To formally evaluate its effectiveness, the rate process-based theoretical model proposed herein was incorporated into a multiphase 1D numerical framework to simulate the progression of BEP. Three independent tests, with different seepage conditions and specimen sizes, were simulated. Three-dimensional seepage flow conditions were shown to influence the simulation of BEP (Vandenboer *et al*., 2018). However, as demonstrated by the simulations of experiments performed on 3D set-up (Vandenboer *et al*., 2019; Pol *et al*., 2022), the observed pipe progression rates were well captured by the proposed framework. Moreover, the values of activation energy and number of bonds per area calibrated with data from independent works are in good agreement with each other, and align with the values estimated from the regression analysis. The numerical results are in good agreement with the experimental observations in both the evolution of local gradients and BEP progression rates. The reported results indicate that the proposed constitutive model brings the potential to be embedded in high-fidelity 3D numerical frameworks, which is the focus of ongoing research work. The proposed model could also be employed in numerical investigations to provide assessment of BEP risk and prediction of survivability of flood protection systems under dynamic hydraulic loading conditions.

NOTATION

D	diffusivity
E_{flow}	flow energy
$\bar{E}_{\text{flow}}$	flow energy density
f	force
h	hydraulic head
h_{b}	boundary hydraulic head
h_{p}	Planck's constant
k	hydraulic conductivity
k_{b}	Boltzmann's constant
m_{fu}	average mass of flow unit
N	Avogadro constant
$\boldsymbol{n}_{\text{i}}$	outer unit normal vector of inlet boundary
$\boldsymbol{n}_{\text{o}}$	outer unit normal vector of outlet boundary
$\bar{n}$	average number of flow units per unit volume
P_{flow}	flow power
$\bar{P}_{\text{flow}}$	flow power density
p	static hydraulic pressure
q	outward flux
q_{b}	boundary flux
R	universal gas constant
S	number of bonds per unit area
S_{i}	inlet boundary surface
S_{o}	outlet boundary surface
S_{s}	specific storage
T	absolute temperature
V	control volume
V_{f}	average volume of flow unit
$\boldsymbol{v}$	flow velocity
z	elevation
α	erosion model parameter 1
β	erosion model parameter 2
γ	concentration of fluidised particles
γ_{w}	unit weight of water
ΔF	activation energy
λ	distance between successive equilibrium positions
ν	frequency of activation
ρ_{dry}	dry bulk density
ρ_{s}	density of soil particle
ϕ	porosity
ϕ_{lim}	limit porosity

REFERENCES

Albalasmeh, A. A. & Ghezzehei, T. A. (2014). Interplay between soil drying and root exudation in rhizosheath development. *Plant Soil* **374**, 739–751, https://doi.org/10.1007/s11104-013-1910-y.

Andersland, O. & Douglas, A. (1970). Soil deformation rates and activation energies. *Géotechnique* **20**, No. 1, 1–16, https://doi.org/10.1680/geot.1970.20.1.1.

ASTM (2016). D4254-16: standard test methods for minimum index density and unit weight of soils and calculation of relative density, https://doi.org/10.1520/D4254-16. West Conshohocken, PA, USA: ASTM International.

Bagnold, R. A. (1980). An empirical correlation of bedload transport rates in flumes and natural rivers. *Proc. R. Soc. Lond. A. Math. Phys. Sci.* **372**, No. 1751, 453–473, https://doi.org/10.1098/rspa.1980.0122.

Bligh, W. G. (1910). Dams, barrages and weirs on porous foundations. *Engng News* **64**, No. 26, 708–710.

Brandon, T. L., Batool, A., Jimenez, M., Vroman, N. D. & Corcoran, M. K. (2018). Comparison of levee underseepage analysis methods using blanket theory and finite element analysis, https://doi.org/10.21079/11681/28472. Vicksburg, MS, USA: US Army Engineer Research and Development Center, Geotechnical and Structures Laboratory.

Christensen, R. W. & Das, B. M. (1973). *Hydraulic erosion of remolded cohesive soils*. Highway Research Board Special Report No. 135. Washington, DC, USA: Transportation Research Board.

El Shamy, U. & Aydin, F. (2008). Multiscale modeling of flood-induced piping in river levees. *J. Geotech. Geoenviron. Engng* **134**, No. 9, 1385–1398, https://doi.org/10.1061/(asce)1090-0241(2008)134:9(1385).

Eyring, H. (1936). Viscosity, plasticity, and diffusion as examples of absolute reaction rates. *J. Chem. Phys.* **4**, No. 4, 283–291, https://doi.org/10.1063/1.1749836.

Fascetti, A. & Oskay, C. (2019a). Dual random lattice modeling of backward erosion piping. *Comput. Geotech.* **105**, 265–276, https://doi.org/10.1016/j.compgeo.2018.08.018.

Fascetti, A. & Oskay, C. (2019b). Multiscale modeling of backward erosion piping in flood protection system infrastructure. *Comput.-aided Civ. Infrastruct. Engng* **34**, No. 12, 1071–1086, https://doi.org/10.1111/mice.12489.

Fleshman, M. S. & Rice, J. D. (2013). Constant gradient piping test apparatus for evaluation of critical hydraulic conditions for the initiation of piping. *Geotech. Test. J.* **36**, No. 6, 834–846, https://doi.org/10.1520/gtj20130066.

Fleshman, M. S. & Rice, J. D. (2014). Laboratory modeling of the mechanisms of piping erosion initiation. *J. Geotech. Geoenviron. Engng* **140**, No. 6, 04014017, https://doi.org/10.1061/(asce)gt.1943-5606.0001106.

Foster, M., Fell, R. & Spannagle, M. (2000). The statistics of embankment dam failures and accidents. *Can. Geotech. J.* **37**, No. 5, 1000–1024, https://doi.org/10.1139/t00-030.

Gelet, R. & Marot, D. (2022). Internal erosion by suffusion on cohesionless gap-graded soils: model and sensibility analysis. *Geomech. Energy Environ.* **31**, 100313, https://doi.org/10.1016/j.gete.2022.100313.

Glasstone, S., Laidler, K. J. & Eyring, H. (1941). *The theory of rate process: the kinetics of chemical reactions, viscosity, diffusion and electrochemical phenomena*. New York, USA and London, UK: McGraw-Hill Book Company, Inc.

Govers, G. (1992). Evaluation of transporting capacity formulae for overland flow. In *Overland flow* (eds A. J. Parsons and A. D. Abrahamls), pp. 224–261, https://doi.org/10.1201/b12648-17. London, UK: CRC Press.

Gularte, R. C., Kelly, W. & Nacci, V. (1980). Erosion of cohesive sediments as a rate process. *Ocean Engng* **7**, No. 4, 539–551, https://doi.org/10.1016/0029-8018(80)90051-7.

ICOLD (International Commission on Large Dams) (2013). *ICOLD Bulletin 164 on internal erosion of dams, dikes and levees and their foundations*. Paris, France: International Commission on Large Dams.

Kodieh, A., Gelet, R., Marot, D. & Fino, A. (2021). A study of suffusion kinetics inspired from experimental data: comparison of three different approaches. *Acta Geotech.* **16**, 347–365, https://doi.org/10.1007/s11440-020-01016-5.

Kuang, X., Jiao, J. J., Zheng, C., Cherry, J. A. & Li, H. (2020). A review of specific storage in aquifers. *J. Hydrol.* **581**, 124383, https://doi.org/10.1016/j.jhydrol.2019.124383.

Marchi, M., Martínez, M. F. G., Gottardi, G. & Tonni, L. (2021). Field measurements on a large natural sand boil along the river

Po, Italy. *Q. J. Engng Geol. Hydrogeol.* **54**, No. 4, qjegh2020-097, https://doi.org/10.1144/qjegh2020-097.
Marot, D., Le, V. D., Garnier, J., Thorel, L. & Audrain, P. (2012). Study of scale effect in an internal erosion mechanism: centrifuge model and energy analysis. *Eur. J. Environ. Civ. Engng* **16**, No. 1, 1–19, https://doi.org/10.1080/19648189.2012.667203.
Matsui, T., Abe, N., Mitchell, J. K. & Ito, T. (1980). Microscopic study of shear mechanisms in soils. *J. Geotech. Engng Div.* **106**, No. 2, 137–152, https://doi.org/10.3208/sandf1972.14.29.
Michalowski, R., Wang, Z. & Nadukuru, S. (2018). Maturing of contacts and ageing of silica sand. *Géotechnique* **68**, No. 2, 133–145, https://doi.org/10.1680/jgeot.16.p.321.
Mitchell, J. K. (1964). Shearing resistance of soils as a rate process. *J. Soil Mech. Found. Div.* **90**, No. 1, 29–61, https://doi.org/10.1016/0022-4898(64)90023-0.
Mitchell, J. K. & Soga, K. (2005). *Fundamentals of soil behavior*. Hoboken, NJ, USA: John Wiley & Sons.
Mitchell, J. K., Campanella, R. G. & Singh, A. (1968). Soil creep as a rate process. *J. Soil Mech. Found. Div.* **94**, No. 1, 231–253, https://doi.org/10.1061/jsfeaq.0001085.
Mitchell, J. K., Singh, A. & Campanella, R. G. (1969). Bonding, effective stresses, and strength of soils. *J. Soil Mech. Found. Div.* **95**, No. 5, 1219–1246, https://doi.org/10.1016/0022-4898(70)90065-0.
Murayama, S. & Shibata, T. (1961). Rheological properties of clays. *Proceedings of the 5th international conference on soil mechanics and foundation engineering (ICSMFE), Paris, France* (ed A. Caquot), pp. 269–273. Paris, France: Dunod.
Murayama, S., Michihiro, K. & Sakagami, T. (1984). Creep characteristics of sands. *Soils Found.* **24**, No. 2, 1–15, https://doi.org/10.3208/sandf1972.24.2_1.
Negrinelli, G. (2015). *Investigation of the process of seepage and backward erosion piping under dikes in heterogeneous sands*. PhD thesis, University of Brescia, Brescia, Italy.
Negrinelli, G., van Beek, V. & Ranzi, R. (2016). Experimental and numerical investigation of backward erosion piping in heterogeneous sands. In *Scour and erosion: proceedings of the 8th international conference on scour and erosion* (eds J. Harris, R. Whitehouse and S. Moxon), pp. 473–482. Leiden, The Netherlands: CRC Press/Balkema.
Ojha, C., Singh, V. & Adrian, D. (2003). Determination of critical head in soil piping. *J. Hydr. Engng* **129**, No. 7, 511–518, https://doi.org/10.1061/(asce)0733-9429(2003)129:7(511).
Ovalle-Villamil, W. & Sasanakul, I. (2021). Centrifuge modeling study of backward erosion piping with variable exit size. *J. Geotech. Geoenviron. Engng* **147**, No. 11, 04021114, https://doi.org/10.1061/(asce)gt.1943-5606.0002642.
Papamichos, E. & Vardoulakis, I. (2005). Sand erosion with a porosity diffusion law. *Comput. Geotech.* **32**, No. 1, 47–58, https://doi.org/10.1016/j.compgeo.2004.11.005.
Peng, S. & Rice, J. D. (2020). Measuring critical gradients for soil loosening and initiation of backward erosion-piping mechanism. *J. Geotech. Geoenviron. Engng* **146**, No. 8, 04020069, https://doi.org/10.1061/(ASCE)GT.1943-5606.0002277.
Pol, J. C., Kanning, W., van Beek, V. M., Robbins, B. A. & Jonkman, S. N. (2022). Temporal evolution of backward erosion piping in small-scale experiments. *Acta Geotech.* **17**, No. 10, 4555–4576, https://doi.org/10.1007/s11440-022-01545-1.
Powell, T. & Richerson, P. J. (1985). Temporal variation, spatial heterogeneity, and competition for resources in plankton systems: a theoretical model. *Am. Nat.* **125**, No. 3, 431–464, https://doi.org/10.1086/284352.
Raudkivi, A. & Hutchison, D. (1974). Erosion of kaolinite clay by flowing water. *Proc. R. Soc. Lond. A. Math. Phys. Sci.* **337**, No. 1611, 537–554, https://doi.org/10.1098/rspa.1974.0066.
Reddi, L. N., Bonala, M. & Lee, I. (2000). Comparison of internal and surface erosion using flow pump tests on a sand-kaolinite mixture. *Geotech. Test. J.* **23**, No. 1, 116–122, https://doi.org/10.1520/gtj11129j.
Richards, K. S. & Reddy, K. R. (2007). Critical appraisal of piping phenomena in earth dams. *Bull. Engng Geol. Environ.* **66**, 381–402, https://doi.org/10.1007/s10064-007-0095-0.
Richards, K. S. & Reddy, K. R. (2012). Experimental investigation of initiation of backward erosion piping in soils. *Géotechnique* **62**, No. 10, 933–942, https://doi.org/10.1680/geot.11.p.058.
Riha, J. & Petrula, L. (2023). Experimental research on backward erosion piping progression. *Water* **15**, No. 15, 2749, See https://www.mdpi.com/2073-4441/15/15/2749.
Robbins, B. A. (2016). Numerical modeling of backward erosion piping. In *The 4th Itasca symposium on applied numerical modeling, Lima, Peru* (eds P. Gómez, C. Detournay, R. Hart and M. Nelson), pp. 551–558. Minneapolis, MN, USA: Itasca International Inc.
Robbins, B. & Griffiths, D. (2021). A two-dimensional, adaptive finite element approach for simulation of backward erosion piping. *Comput. Geotech.* **129**, 103820, https://doi.org/10.1016/j.compgeo.2020.103820.
Robbins, B. A., van Beek, V. M., López-Soto, J. F., Montalvo-Bartolomei, A. M. & Murphy, J. (2018). A novel laboratory test for backward erosion piping. *Int. J. Phys. Model. Geotech.* **18**, No. 5, 266–279, https://doi.org/10.1680/jphmg.17.00016.
Robbins, B. A., Stephens, I. J., Van Beek, V. M., Koelewijn, A. R. & Bezuijen, A. (2020). Field measurements of sand boil hydraulics. *Géotechnique* **70**, No. 2, 153–160, https://doi.org/10.1680/jgeot.18.p.151.
Sail, Y., Marot, D., Sibille, L. & Alexis, A. (2011). Suffusion tests on cohesionless granular matter: experimental study. *Eur. J. Environ. Civ. Engng* **15**, No. 5, 799–817, https://doi.org/10.1080/19648189.2011.9693366.
Saltelli, A., Ratto, M., Andres, T., Campolongo, F., Cariboni, J., Gatelli, D., Saisana, M. & Tarantola, S. (2008). *Global sensitivity analysis: the primer*. Chichester, UK: John Wiley & Sons.
Schmertmann, J. H. (2000). The no-filter factor of safety against piping through sands. In *Judgment and innovation: the heritage and future of the geotechnical engineering profession* (eds F. Silva and E. Kavazanjian Jr), pp. 65–132, https://doi.org/10.1061/9780784405376.006. Reston, VA, USA: American Society of Civil Engineers.
Sellmeijer, H., de la Cruz, J. L., van Beek, V. M. & Knoeff, H. (2011). Fine-tuning of the backward erosion piping model through small-scale, medium-scale and IJkdijk experiments. *Eur. J. Environ. Civ. Engng* **15**, No. 8, 1139–1154, https://doi.org/10.1080/19648189.2011.9714845.
Sellmeyer, J. B. (1988). *On the mechanism of piping under impervious structures*. PhD thesis, Delft University of Technology, Delft, Netherlands.
Sibille, L., Lominé, F., Poullain, P., Sail, Y. & Marot, D. (2015). Internal erosion in granular media: direct numerical simulations and energy interpretation. *Hydrol. Processes* **29**, No. 9, 2149–2163, https://doi.org/10.1002/hyp.10351.
Sterpi, D. (2003). Effects of the erosion and transport of fine particles due to seepage flow. *Int. J. Geomech.* **3**, No. 1, 111–122, https://doi.org/10.1061/(asce)1532-3641(2003)3:1(111).
Teunissen, P. J. G. (1990). Nonlinear least squares. *Manuscr. Geod.* **15**, 137–150.
Thomas, J. W. (2013). *Numerical partial differential equations: finite difference methods*. New York, NY, USA: Springer.
van Beek, V. M. (2015). *Backward erosion piping: initiation and progression*. PhD thesis, Delft University of Technology, Delft, Netherlands.
van Beek, V. M., De Bruijn, H., Knoeff, J., Bezuijen, A. & Förster, U. (2010). Levee failure due to piping: a full-scale experiment. In *Proceedings of 5th international conference on scour and erosion (ICSE-5), San Francisco, CA, USA* (eds S. E. Burns, S. K. Bhatia, C. M. C. Avila and B. E. Hunt), pp. 283–292, https://doi.org/10.1061/41147(392)27. Reston, VA, USA: American Society of Civil Engineers.
van Beek, V. M., Knoeff, H. & Sellmeijer, H. (2011). Observations on the process of backward erosion piping in small-, medium-and full-scale experiments. *Eur. J. Environ. Civ. Engng* **15**, No. 8, 1115–1137, https://doi.org/10.1080/19648189.2011.9714844.
van Beek, V., Van Essen, H., Vandenboer, K. & Bezuijen, A. (2015). Developments in modelling of backward erosion piping. *Géotechnique* **65**, No. 9, 740–754, https://doi.org/10.1680/geot.14.p.119.
Vandenboer, K., van Beek, V. & Bezuijen, A. (2014). 3D Finite element method (FEM) simulation of groundwater flow during backward erosion piping. *Front. Struct. Civ. Engng* **8**, 160–166, https://doi.org/10.1007/s11709-014-0257-7.

Vandenboer, K., Van Beek, V. & Bezuijen, A. (2018). 3D Character of backward erosion piping. *Géotechnique* **68**, No. 1, 86–90, https://doi.org/10.1680/jgeot.16.p.091.

Vandenboer, K., Celette, F. & Bezuijen, A. (2019). The effect of sudden critical and supercritical hydraulic loads on backward erosion piping: small-scale experiments. *Acta Geotech.* **14**, 783–794, https://doi.org/10.1007/s11440-018-0756-0.

Wang, Z. (2017). *Contact maturing and aging of silica sand*. PhD thesis, University of Michigan, Ann Arbor, MI, USA.

Wang, Y. & Ni, X. (2013). Hydro-mechanical analysis of piping erosion based on similarity criterion at micro-level by PFC3D. *Eur. J. Environ. Civ. Engng* **17**, No. sup1, s187–s204, https://doi.org/10.1080/19648189.2013.834594.

White, F. M. (1999). Open channel flow. In *Fluid mechanics* (ed. F. Kreith), pp. 65–73. Boca Raton, FL, USA: CRC Press.

Zhang, X., Wong, H., Leo, C. J., Bui, T. A., Wang, J., Sun, W. & Huang, Z. (2013). A thermodynamics-based model on the internal erosion of earth structures. *Geotech. Geol. Engng* **31**, 479–492, https://doi.org/10.1007/s10706-012-9600-8.